VIP Batteries Very Important Paper

How to cite:
International Edition: doi.org/10.1002/anie.202008634
German Edition: doi.org/10.1002/ange.202008634

Hydrophobic Organic-Electrolyte-Protected Zinc Anodes for Aqueous Zinc Batteries

*Longsheng Cao[+], Dan Li[+], Tao Deng, Qin Li, and Chunsheng Wang**

Abstract: *Aqueous Zn batteries are promising energy-storage devices. However, their lifespan is limited by irreversible Zn anodes owing to water decomposition and Zn dendrite growth. Here, we separate aqueous electrolyte from Zn anode by coating a thin MOF layer on anode and filling the pores of MOF with hydrophobic $Zn(TFSI)_2$-tris(2,2,2-trifluoroethyl)-phosphate (TFEP) organic electrolyte that is immiscible with aqueous $Zn(TFSI)_2$–H_2O bulk electrolyte. The MOF encapsulated $Zn(TFSI)_2$-TFEP forms a ZnF_2-$Zn_3(PO_4)_2$ solid electrolyte interphase (SEI) preventing Zn dendrite and water decomposition. The $Zn(TFSI)_2$-TFEP@MOF electrolyte protected Zn anode enables a Zn || Ti cell to achieve a high average Coulombic efficiency of 99.1 % for 350 cycles. The highly reversible Zn anode brings a high energy density of 210 Wh kg^{-1} (of cathode and anode mass) and a low capacity decay rate of 0.0047 % per cycle over 600 cycles in a Zn || MnO_2 full cell with a low capacity ratio of Zn:MnO_2 at 2:1.*

Introduction

Aqueous zinc batteries have attracted extensive attention owing to the high theoretical capacities (820 mAh g^{-1} or 5855 mAh cm^{-3}), low cost, and environmental friendliness.[1] Aqueous electrolyte overcomes strong cation–anion association, suppresses electrostatic repulsion between ions, and facilitates rapid diffusion kinetics of ions by water shielding effect in bulk electrolyte.[2] However, the reaction of Zn anodes with water in aqueous electrolytes brings challenge by forming a passivated solid layer on Zn, resulting in a low CE of zinc plating/stripping, Zn dendrite growth, and quick short circuiting.[1a,2a,b,3]

Solvated Zn^{2+} brings water into the electric double layer, resulting in parasitic water reduction during Zn deposition since water is thermodynamically unstable in the Zn deposition potential. (Figure 1 a).[4,5] The formation of H_2 by water reduction changes the local pH value.[5] Subsequently, the emerging strong alkaline environment would corrode the Zn surface and initiate the formation of $Zn(OH)_2$ and ZnO. The H_2 evolution in aqueous electrolyte also inevitably induces substantial fluctuation in the micro-environment. To significantly minimize the water reduction from solvated $[Zn(H_2O)_6]^{2+}$ species, Wang et al.[1a] introduced saturated electrolytes (water-in-salt) to reduce $[Zn(H_2O)_6]^{2+}$ species. In 21 m LiTFSI-H_2O-1.0 m $Zn(TFSI)_2$ water-in-salt electrolyte, Zn^{2+} are closely coordinated with $TFSI^-$ in pairs rather than H_2O, and the H_2O activity in electrolyte is significantly reduced. Therefore, the water decomposition is avoided during Zn deposition. However, the high cost and viscosity of the water-in-salt electrolytes remain unsolved. Another approach is to coat a dense hydrophobic solid organic polyamide interphase layer to suppress water penetration and decomposition.[6] However, the artificial coating layer lacks self-repair capability, limiting the cycle life of Zn anodes. To enhance the reversibility of Zn anode, the water content on the Zn surface should be minimized and a self-repaired solid electrolyte interphase (SEI) should be formed in situ on Zn anodes.

Here, we separate the Zn anode from 1.0 M $Zn(TFSI)_2$-H_2O aqueous electrolyte by coating a circa 1.0 μm MOF layer on Zn and then infiltrate 1.0 M $Zn(TFSI)_2$-tris(2,2,2-trifluoroethyl)phosphate (TFEP) organic electrolyte into the pores of organophilic MOF. $Zn(TFSI)_2$-TFEP organic electrolyte is immiscible with $Zn(TFSI)_2$-H_2O electrolyte preventing H_2O from penetrating to Zn surface (Figure 1 b). $Cu_3(BTC)_2$ (HKUST-1) MOF has three-dimensional channel structure with highly ordered micropores of approximately 9 Å,[7] enabling TFEP solvent (< 6.6 Å)[8] and Zn^{2+} (0.74 Å) to completely infiltrate into the micropores. At Zn deposition potential, $Zn(TFSI)_2$-TFEP electrolyte is reduced forming self-repaired ZnF_2-$Zn_3(PO_4)_2$ SEI with a high Zn^{2+} conductivity. Since the MOF confined $Zn(TFSI)_2$-TFEP organic electrolyte is immiscible with 1.0 M $Zn(TFSI)_2$-H_2O aqueous electrolyte, solvated H_2O around Zn^{2+} will be replaced by TFEP during Zn^{2+} transport from $Zn(TFSI)_2$-H_2O bulk aqueous electrolyte to $Zn(TFSI)_2$-TFEP organic electrolyte. Even if trace residual solvated H_2O exists in $Zn(TFSI)_2$-TFEP organic electrolyte, it will be completely removed by the

[*] Dr. L. Cao,[+] Dr. D. Li,[+] T. Deng, Q. Li, Prof. C. Wang
Department of Chemical and Biomolecular Engineering
University of Maryland, College Park, MD 20742 (USA)
E-mail: cswang@umd.edu
Prof. C. Wang
Department of Chemistry and Biochemistry
University of Maryland, College Park, MD 20742 (USA)
[+] These authors contributed equally to this work.
Supporting information and the ORCID identification number(s) for the author(s) of this article can be found under: https://doi.org/10.1002/anie.202008634.

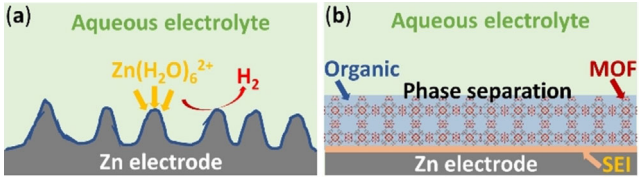

Figure 1. Illustration of the surface structure and surface reaction of Zn anodes. a) Water side reaction and Zn dendrite formation on Zn foil. b) SEI formation in MOF confined organic electrolyte that is immiscible with aqueous electrolyte.

ZnF_2-$Zn_3(PO_4)_2$ SEI layer. The SEI/$Zn(TFSI)_2$-TFEP bi-layer significantly enhanced the Zn plating/stripping CE to 99.9% and Zn dendrite-free cycles for up to 700 h. The Zn||MnO_2 batteries remain 97.2% of initial capacity after 600 cycles.

Results and Discussion

Characterization and Properties of MOF-Encapsulated $Zn(TFSI)_2$-TFEP Electrolyte

Based on X-ray diffraction (XRD; Figure 2a) and scanning electron microscopy (SEM; Figure 2b), HKUST-1 MOF shows well-crystalline structure and a uniform particle size of about 0.5 μm, consistent with the reported MOF.[9] After the MOF layer coating, light silver of Zn electrode changes to cyan-blue (Figure 2c). To obtain the thickness of MOF coating, the MOF coated Zn foil was partially scratched as shown in SEM image (Figure 2d). MOF layer with thickness of about 1.0 μm is tightly adhered to the Zn surface. Since MOF is organophilic and has continues three-dimensional nano-pores, $Zn(TFSI)_2$-TFEP can easily be infiltrated and confined inside MOF to protect Zn. The selection of $Zn(TFSI)_2$-TFEP to protect Zn is because it is immiscible with (phase separation from) aqueous $Zn(TFSI)_2$-H_2O electrolyte, as evidenced by a clear interface between the organic $Zn(TFSI)_2$-TFEP electrolyte (in the bottom) and the aqueous $Zn(TFSI)_2$-H_2O electrolyte (on the top) in Figure 2e. At the organic/water interface, the solvated H_2O around Zn^{2+} is exchanged by the TFEP, successfully preventing the side reactions of water with Zn.

The electrochemical stability windows of $Zn(TFSI)_2$-H_2O aqueous electrolyte and phase separated 1.0 M $Zn(TFSI)_2$-TFEP@MOF/1.0 M $Zn(TFSI)_2$-H_2O (denoted as $Zn(TFSI)_2$-TFEP@MOF/H_2O) electrolytes were evaluated on non-active Ti electrode after five formation cycles using cyclic voltammetry (CV). As shown in the Supporting Information, Figure S1, during the cathodic scan in $Zn(TFSI)_2$-H_2O electrolyte, water begins to reduce at 0.16 V, followed by Zn deposition at −0.04 V, while the water reduction current in the $Zn(TFSI)_2$-TFEP@MOF/H_2O electrolyte is complexly suppressed, and Zn starts to deposit at −0.075 V. Therefore, the water reduction on Zn is eliminated in $Zn(TFSI)_2$-TFEP@MOF/H_2O bi-layer hybrid electrolyte. The thermal stabilities of TFEP, $Zn(TFSI)_2$-TFEP, MOF, and $Zn(TFSI)_2$-TFEP@MOF were evaluated using thermal gravity analysis (TGA). The addition of $Zn(TFSI)_2$ into TFEP effectively suppresses the TFEP evaporation by increasing evaporation starting temperature (EST) from 101 to 132 °C, due to strong solvation effect (Supporting Information, Figure S2a,b). Moreover, the presence of MOF further stabilizes the TFEP increasing EST to 198 °C, due to the strong interaction between MOF and organic electrolyte (Supporting Information, Figure S2c,d). This interaction contributes to localizing the electrolyte on electrode surface.

Electrochemical Performance of the Zn Anode in $Zn(TFSI)_2$-TFEP@MOF/H_2O Electrolyte

The Zn plating/stripping stability in different electrolytes was evaluated using Zn||Zn symmetric cells at 0.5 mA cm^{-2} and 0.5 mAh cm^{-2} (Figure 3a). The Zn symmetric cell using the $Zn(TFSI)_2$-TFEP@MOF/H_2O electrolyte shows high

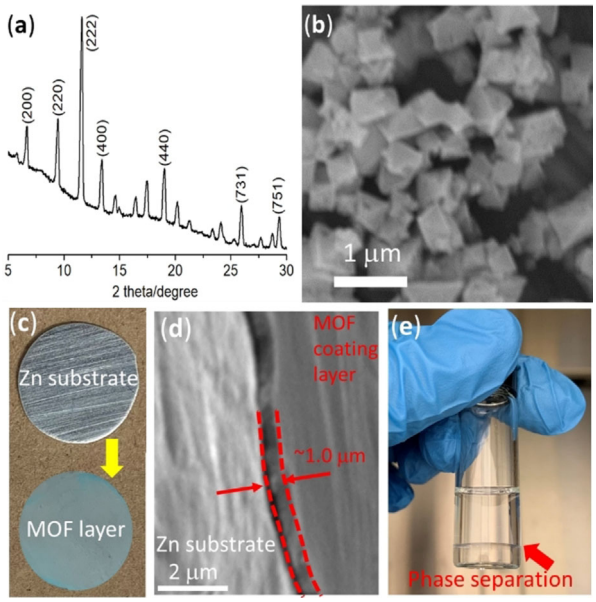

Figure 2. a) XRD patterns and b) SEM image of MOF. c) Photographs of the zinc electrode before and after surface coating of MOF layer. d) SEM image of MOF partially-coated Zn electrode; the coated MOF was scratched on the left side to measure the coating thickness (ca. 1.0 μm) e) Phase separation of 1.0 M $Zn(TFSI)_2$-H_2O (on the top) from 1.0 M $Zn(TFSI)_2$-TFEP (on the bottom). A clear interface between two electrolytes is observed.

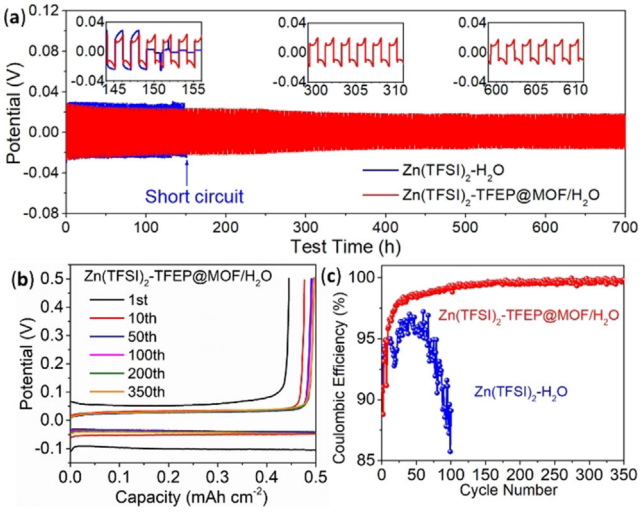

Figure 3. a) Galvanostatic Zn plating/stripping in Zn||Zn symmetrical cells at 0.5 mA cm^{-2} and 0.5 mAh cm^{-2}. b) Voltage profiles of Zn plating/stripping processes at selected cycles in $Zn(TFSI)_2$-TFEP@MOF/H_2O electrolyte. c) Zn plating/stripping CE in different electrolytes.

reversibility and stability over 700 h, while Zn symmetric cell using the $Zn(TFSI)_2$-H_2O reference electrolyte shorts after only 150 h. Furthermore, the Zn symmetric cell using Zn-$(TFSI)_2$-TFEP@MOF/H_2O electrolyte shows gradually decreased overpotential and eventually stabilizes at about 20 mV, which is much smaller than that using $Zn(TFSI)_2$-H_2O electrolyte (ca. 30 mV). Therefore, the $Zn(TFSI)_2$-TFEP@MOF/H_2O electrolyte successfully suppresses Zn dendrite growth and reduces the Zn plating/stripping polarization.

The mechanism for polarization reduction in $Zn(TFSI)_2$-TFEP@MOF/H_2O electrolytes was investigated using electrochemical impedance spectroscopy (EIS). From the EIS of Zn symmetric cells after 100 cycles (Supporting Information, Figure S3), the impedance of Zn||Zn symmetric cell in $Zn(TFSI)_2$-H_2O electrolytes (blue line) shows a larger resistance than the cell using $Zn(TFSI)_2$-TFEP@MOF/H_2O electrolytes, suggesting the ZnO layer form in $Zn(TFSI)_2$-H_2O electrolyte is more resistive than the SEI formed in organic electrolyte.

Furthermore, even when the cycling current is reduced to 0.1 mA cm^{-2}, the Zn||Zn symmetric cell using $Zn(TFSI)_2$-TFEP organic electrolyte still shows a high zinc plating/stripping overpotential of about 500 mV, more than twenty times higher than that using $Zn(TFSI)_2$-TFEP@MOF/H_2O at 0.5 mA cm^{-2} (Supporting Information, Figure S4). Although Zn-ion conductivity (1.1 mS cm^{-1}) of the 1.0 M $Zn(TFSI)_2$-TFEP organic electrolyte is lower than that (35.9 mS cm^{-1}) of 1.0 M $Zn(TFSI)_2$-H_2O aqueous electrolyte, an extra-thin (ca. 1.0 μm) layer of $Zn(TFSI)_2$-TFEP has significantly reduced the Zn-ion transport resistance. The reaction kinetics of Zn anodes in $Zn(TFSI)_2$-TFEP@MOF/H_2O and $Zn(TFSI)_2$-H_2O electrolytes were also compared in more aggressive protocol of a step-increased current density but a fixed capacity of 3 mAh cm^{-2}. As shown in the Supporting Information, Figure S5, both cells show a similar increase in overpotential of Zn plating/stripping when the current density increases from 4 to 46 mA cm^{-2}, confirming that the thin organic electrolyte layer coating did not reduce the reaction kinetics even at a high current density of 46 mA cm^{-2}, which lays the foundation for designing high-rate Zn batteries. To build a high energy Zn battery, a high areal capacity is required. The cycling stability of Zn anode at an extremely high areal capacity of 10 mAh cm^{-2} was evaluated. At a low current of 0.5 mA cm^{-2} and 10 mAh cm^{-2} (charge/discharge interval being extended to 20 h; Supporting Information, Figure S6a), the Zn||Zn cells in $Zn(TFSI)_2$-TFEP@MOF/H_2O electrolyte remain stable with smaller polarization than that in Zn-$(TFSI)_2$-H_2O electrolyte, while the overpotential of Zn||Zn cells in the later continuously increases in each charge/discharge process. As the current density was further increased to 10 mA cm^{-2} at 10 mAh cm^{-2} (Supporting Information, Figure S6b), Zn plating/stripping in $Zn(TFSI)_2$-TFEP@MOF/H_2O electrolyte still maintained superior reaction kinetics and impressive stability without voltage fluctuation. In contrast, an erratic voltage response with the rapidly rising overpotential occurred after only 150 mAh cm^{-2} and short circuit happened after 250 mAh cm^{-2} in $Zn(TFSI)_2$-H_2O electrolyte.

The Zn plating/stripping CE in two electrolytes was investigated using Zn||Ti cells at 1 mA cm^{-2} and 0.5 mAh cm^{-2}. The Zn CE is defined as the ratio of the stripped capacity to the plated capacity. The behaviors of zinc plating/stripping on Ti in $Zn(TFSI)_2$-TFEP@MOF/H_2O and $Zn(TFSI)_2$-H_2O electrolytes are shown in Figure 3b and the Supporting Information, Figure S7, respectively. Zn||Ti cell in $Zn(TFSI)_2$-TFEP@MOF/H_2O electrolytes showed a stable Zn plating/stripping overpotential with gradually increased stripping capacity (Figure 3b; Supporting Information, Figure S7a), while the Zn||Ti cell in $Zn(TFSI)_2$-H_2O electrolyte fails quickly after 90 cycles (Supporting Information, Figure S7b,c). The Zn plating/stripping CEs in two electrolytes are compared in Figure 3c. The CE in $Zn(TFSI)_2$-TFEP@-MOF/H_2O electrolyte quickly increased to $>99.0\%$ within 80 cycles, further increased to 99.5% after 130 cycles and finally stabilized at 99.9% after 300 cycle, similar to that in 1.0 M $Zn(TFSI)_2$-TFEP organic electrolytes (Supporting Information, Figure S8). In contrast, the CE in $Zn(TFSI)_2$-H_2O electrolyte reached 96% at 50 cycles and quickly dropped after 90 cycles. Therefore, MOF-confined organic electrolyte layer effectively suppresses side reactions between Zn and water. The Zn||Ti half-cell using $Zn(TFSI)_2$-TFEP@MOF/H_2O electrolyte also has a much lower resistance than that in $Zn(TFSI)_2$-H_2O electrolyte (Supporting Information, Figure S9).

The zinc electrode surface morphologies after 100 plating/stripping cycles are characterized using SEM (Figure 4). After 100 cycles, the Zn surface in $Zn(TFSI)_2$-H_2O electrolyte become porous structure with needle-like dendrite (Figure 4a–c) owing to continuous reactions between Zn and electrolyte, as evidenced by a low CE ($<96\%$) and poor cycling stability. In contrast, the plated Zn in $Zn(TFSI)_2$/TFEP@MOF/H_2O electrolyte shows a dense and smooth morphology (Figure 4d–f), confirmed by uniform F and P elements distribution (Supporting Information, Figure S10). The thickness of the cycled Zn in $Zn(TFSI)_2$-H_2O electrolyte is 25 μm, and reduced to 12.5 μm when it was cycled in $Zn(TFSI)_2$/TFEP@MOF/H_2O (red lines in Figure 4c,f). Therefore, MOF-confined hydrophobic $Zn(TFSI)_2$-TFEP

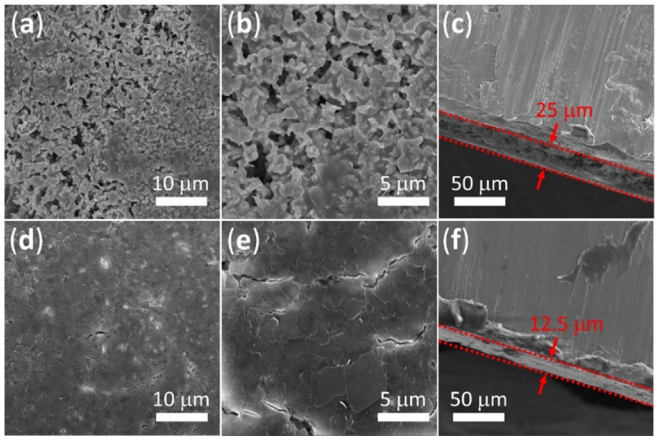

Figure 4. SEM images of Zn electrodes in Zn||Zn symmetrical cells after 100 plating/striping cycles at 0.5 mA cm^{-2} and 0.5 mAh cm^{-2} in $Zn(TFSI)_2$-H_2O (a–c), and $Zn(TFSI)_2$-TFEP@MOF/H_2O (d–f) electrolytes. In (c) and (f), red lines indicated the etching depth.

organic electrolyte layer on Zn surface effectively suppressed water penetration from $Zn(TFSI)_2$-H_2O to Zn surface, which suppressed Zn dendrite growth. Here, water was chemically blocked by hydrophobic $Zn(TFSI)_2$-TFEP organic electrolyte that is immiscible with $Zn(TFSI)_2$-H_2O aqueous electrolytes, rather than physically blocked by a ceramic layer reported before that lacks self-repair capability if it is cracked. The MOF is just to confine $Zn(TFSI)_2$-TFEP organic electrolyte. Furthermore, the $Zn(TFSI)_2$-TFEP was also reduced at Zn plating potential forming a hydrophobic SEI on Zn surface as demonstrated by XPS below, which can further prevent trace water dissolved in $Zn(TFSI)_2$-TFEP electrolyte from reacting with Zn.

SEI Characterization on Zn Anodes

The surface composition of Zn electrodes after 100 cycles was analyzed using XPS facilitated by Ar^+ sputtering (Figure 5; Supporting Information, Figure S11). For the F 1s spectrum in Figure 5, the top surface (before sputtering) of Zn anodes recovered from $Zn(TFSI)_2$/TFEP@MOF/H_2O electrolyte mainly contains organic CF_3 species (94.7%) with minor inorganic ZnF_2 (5.3%). Since TFEP (boiling point 40 °C) should be completely removed from Zn in XPS chamber, the CF_3 species arise from either of incomplete reduction products of $Zn(TFSI)_2$-TFEP or trace $Zn(TFSI)_2$ residue on Zn surface, while ZnF_2 is due to $Zn(TFSI)_2$-TFEP reduction. To contrast, no inorganic ZnF_2 is detected on Zn electrode from $Zn(TFSI)_2$-H_2O electrolyte (Supporting Information, Figure S12). After 300 s sputtering on Zn surface recovered from $Zn(TFSI)_2$/TFEP@MOF/H_2O electrolyte, CF_3 peak disappeared but new peak at 688.0 eV was detected, which corresponded to CF from the reduction of $Zn(TFSI)_2$-TFEP. Upon further sputtering to 1800 s, the inorganic ZnF_2 content increased from 78.1% at 300 s sputtering to 87.5%. Furthermore, for the P 2p spectrum, the top surface (before sputtering) recovered from $Zn(TFSI)_2$-TFEP@MOF/H_2O electrolyte mainly contains organic PO_3, which could arise from incomplete reduction products of TFEP. After 300 s sputtering, organic PO_3 peak disappeared but new inorganic $Zn_3(PO_4)_2$ peak at 134.1 eV appeared. Upon further sputtering to 1800 s, $Zn_3(PO_4)_2$ peak persists. From FTIR and Raman analysis of Zn surface recovered from $Zn(TFSI)_2$/TFEP@-MOF/H_2O electrolyte (Supporting Information, Figure S13), strong P–O bond stretching and bending peaks[10] were detected, further confirming the formation of $Zn_3(PO_4)_2$. $Zn_3(PO_4)_2$ SEI has a high Zn^{2+} conductivity and this has been proved by both experiment[11] and theoretical[12] analysis, also confirmed in the Supporting Information, Figure S3. The dense ZnF_2-$Zn_3(PO_4)_2$ SEI separates Zn surface from trace water dissolved in the $Zn(TFSI)_2$-TFEP organic electrolyte layer but allows Zn^{2+} to diffuse through.

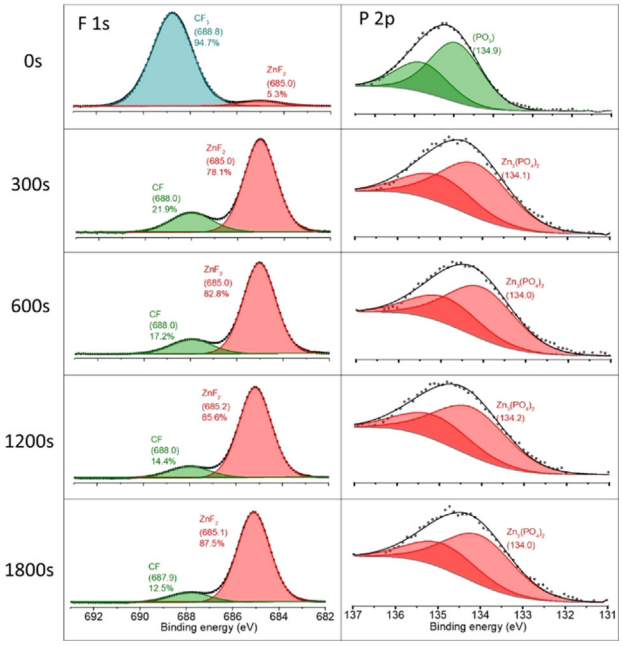

Figure 5. XPS features of the SEI on Zn after 100 charge/discharge cycles in $Zn(TFSI)_2$-TFEP@MOF/H_2O electrolyte. The F 1s and P 2p spectra are displayed in rows, with corresponding Ar^+ sputtering depth profiling results in columns.

Electrochemical Performance of MnO_2 Cathodes and Zn\|\|MnO_2 Full Cells

The $Zn(TFSI)_2$-TFEP protected Zn anode was evaluated in Zn||MnO_2 full cell using tunnel structured β-MnO_2, one of the most promising cathodes with a high theoretical capacity of 308 mAh g^{-1} for aqueous Zn batteries, and compared with that using unprotect Zn in aqueous $Zn(TFSI)_2$-H_2O electrolytes. We first evaluated the electrochemical performance of MnO_2 cathode in two electrolytes using CV at 0.1 mV s^{-1} using a Zn||MnO_2 cells with a high capacity ratio (Zn/MnO_2) of 3.0, and the CV behavior reflects MnO_2 behavior.

As in Figure 6a, MnO_2 in both electrolytes showed the same behavior with distinct Mn-ion redox peaks, consistent

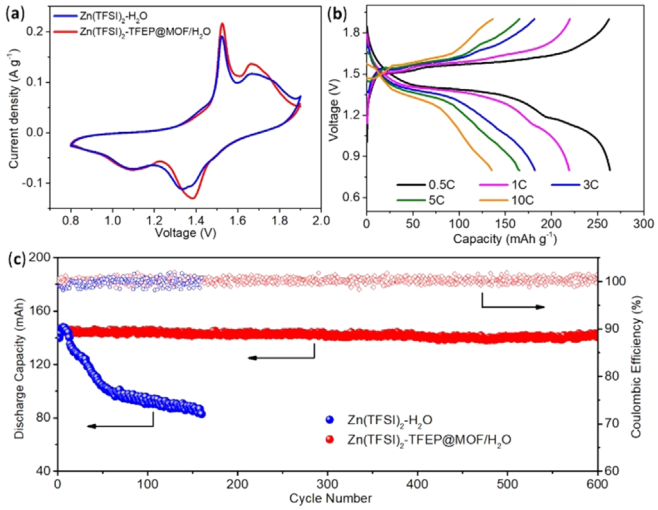

Figure 6. Electrochemical performance of Zn||MnO_2 cells. a) CV of Zn||MnO_2 full cells at a scan rate of 0.1 mV s^{-1}. b) Rate performance in $Zn(TFSI)_2$-TFEP@MOF/H_2O electrolyte. c) Cyclic stability and efficiency of Zn||MnO_2 cells in two electrolytes with 0.1 M $Mn(OTF)_2$ (to suppress Mn^{2+} dissolution) at 10 C.

with the previous work.[13] The rate performance of MnO_2 cells in $Zn(TFSI)_2$-TFEP@MOF/H_2O electrolyte was also evaluated. As in Figure 6b, the MnO_2 cathodes provided a high capacity of 270 $mAh\,g^{-1}$ at a low rate of 0.5 C, and still maintain 135 $mAh\,g^{-1}$ even at a high rate of 10 C. The rate performance in both electrolytes are similar (Supporting Information, Figures S14, S15). At 0.5 C, the capacity based on the (cathode + anode) mass is 154 $mAh\,g^{-1}$, corresponding to an energy density of 210 $Wh\,kg^{-1}$. The long-term cycling stability of the Zn || MnO_2 cell was evaluated at 10 C in both electrolytes with 0.1 M Mn^{2+} additive to suppress Mn^{2+} dissolution (Figure 6c). Even with the capacity ratio of Zn:MnO_2 at 2:1, the Zn || MnO_2 cells after 600 cycles in $Zn(TFSI)_2$-TFEP@MOF/H_2O electrolyte still maintain about 141 $mAh\,g^{-1}$, which is 97.2% of initial capacity with CE approaching 100%, while the capacity of Zn || MnO_2 cells in $Zn(TFSI)_2$-H_2O electrolyte quickly dropped to 59.0% of initial capacity due to low CE for Zn plating/stripping.

Conclusion

Zn dendrite growth and low CE is due to water reduction on Zn anode challenge aqueous Zn batteries. In this work, we separate the $Zn(TFSI)_2$-H_2O aqueous electrolyte from Zn anode by coating a thin (ca. 1.0 μm) hydrophobic $Zn(TFSI)_2$-TFEP organic electrolyte on Zn surface that is immiscible with $Zn(TFSI)_2$-H_2O aqueous electrolyte. To avoid the flow away of hydrophobic $Zn(TFSI)_2$-TFEP organic electrolyte, a thin layer of organophilic MOF was coated on Zn and hydrophobic $Zn(TFSI)_2$-TFEP organic electrolyte was confined inside the MOF pores. MOF confined $Zn(TFSI)_2$-TFEP protecting electrolytes provide several advantages: 1) MOF-confined $Zn(TFSI)_2$-TFEP can chemically prevent water penetration onto Zn anode due to the phase separation of $Zn(TFSI)_2$-TFEP organic electrolyte with $Zn(TFSI)_2$-H_2O aqueous electrolyte, and the formed ZnF_2-$Zn_3(PO_4)_2$ SEI can further block the trace water dissolved in the $Zn(TFSI)_2$-TFEP organic electrolyte layer; 2) ZnF_2-$Zn_3(PO_4)_2$ SEI can be self-repaired if it is broken because it was formed by the reduction of $Zn(TFSI)_2$-TFEP organic electrolytes, which is totally different from ceramic layer coating reported before that is lack of self-repaired capability. $Zn(TFSI)_2$-TFEP protected Zn anodes enabled a Zn anode to achieve a reversible and dendrite-free Zn plating/stripping CE of 99.9%, and Zn || MnO_2 cells with a low capacity ratio of Zn:MnO_2 at 2:1 to achieved a high energy density of 210 $Wh\,kg^{-1}$ (based on cathode and anode) and remained 97.2% of initial capacity after 600 cycles at 10 C.

Conflict of interest

The authors declare no conflict of interest.

Keywords: aqueous zinc batteries · metal–organic frameworks · phase separation · reversibility

[1] a) F. Wang, O. Borodin, T. Gao, X. Fan, W. Sun, F. Han, A. Faraone, J. A. Dura, K. Xu, C. Wang, *Nat. Mater.* **2018**, *17*, 543 – 549; b) L. Ma, S. Chen, N. Li, Z. Liu, Z. Tang, J. A. Zapien, S. Chen, J. Fan, C. Zhi, *Adv. Mater.* **2020**, *32*, 1908121; c) H.-F. Wang, C. Tang, Q. Zhang, *Adv. Funct. Mater.* **2018**, *28*, 1803329.

[2] a) L. E. Blanc, D. Kundu, L. F. Nazar, *Joule* **2020**, *4*, 771 – 799; b) Y. Jin, L. Zou, L. Liu, M. H. Engelhard, R. L. Patel, Z. Nie, K. S. Han, Y. Shao, C. Wang, J. Zhu, H. Pan, J. Liu, *Adv. Mater.* **2019**, *31*, 1900567; c) X. Wu, Y. Xu, C. Zhang, D. P. Leonard, A. Markir, J. Lu, X. Ji, *J. Am. Chem. Soc.* **2019**, *141*, 6338 – 6344.

[3] F. Mo, G. Liang, Q. Meng, Z. Liu, H. Li, J. Fan, C. Zhi, *Energy Environ. Sci.* **2019**, *12*, 706 – 715.

[4] a) J. Yi, P. Liang, X. Liu, K. Wu, Y. Liu, Y. Wang, Y. Xia, J. Zhang, *Energy Environ. Sci.* **2018**, *11*, 3075 – 3095; b) J. J. Hong, L. Zhu, C. Chen, L. Tang, H. Jiang, B. Jin, T. C. Gallagher, Q. Guo, C. Fang, X. Ji, *Angew. Chem. Int. Ed.* **2019**, *58*, 15910 – 15915; *Angew. Chem.* **2019**, *131*, 16057 – 16062.

[5] H. Yang, Z. Chang, Y. Qiao, H. Deng, X. Mu, P. He, H. Zhou, *Angew. Chem. Int. Ed.* **2020**, *59*, 9377 – 9381; *Angew. Chem.* **2020**, *132*, 9463 – 9467.

[6] Z. Zhao, J. Zhao, Z. Hu, J. Li, J. Li, Y. Zhang, C. Wang, G. Cui, *Energy Environ. Sci.* **2019**, *12*, 1938 – 1949.

[7] A. A. Talin, A. Centrone, A. C. Ford, M. E. Foster, V. Stavila, P. Haney, R. A. Kinney, V. Szalai, F. El Gabaly, H. P. Yoon, F. Léonard, M. D. Allendorf, *Science* **2014**, *343*, 66 – 69.

[8] M. Sogawa, S. Sawayama, J. Han, C. Satou, K. Ohara, M. Matsugami, H. Mimura, M. Morita, K. Fujii, *J. Phys. Chem. C* **2019**, *123*, 8699 – 8708.

[9] S. Bai, X. Liu, K. Zhu, S. Wu, H. Zhou, *Nat. Energy* **2016**, *1*, 16094.

[10] a) D. Shakhvorostov, M. H. Müser, N. J. Mosey, D. J. Munoz-Paniagua, G. Pereira, Y. Song, M. Kasrai, P. R. Norton, *J. Chem. Phys.* **2008**, *128*, 074706; b) M. Larzillière, M. E. Jacox, *J. Mol. Spectrosc.* **1980**, *79*, 132 – 150.

[11] W. Shin, J. Lee, Y. Kim, H. Steinfink, A. Heller, *J. Am. Chem. Soc.* **2005**, *127*, 14590 – 14591.

[12] A. Naveed, H. Yang, Y. Shao, J. Yang, N. Yanna, J. Liu, S. Shi, L. Zhang, A. Ye, B. He, J. Wang, *Adv. Mater.* **2019**, *31*, 1900668.

[13] W. Sun, F. Wang, S. Hou, C. Yang, X. Fan, Z. Ma, T. Gao, F. Han, R. Hu, M. Zhu, C. Wang, *J. Am. Chem. Soc.* **2017**, *139*, 9775 – 9778.

Manuscript received: June 19, 2020
Accepted manuscript online: July 7, 2020
Version of record online: ■■ ■■, ■■■■

Research Articles

Batteries

L. Cao, D. Li, T. Deng, Q. Li, C. Wang* ——— ■■■■–■■■■

Hydrophobic Organic-Electrolyte-Protected Zinc Anodes for Aqueous Zinc Batteries

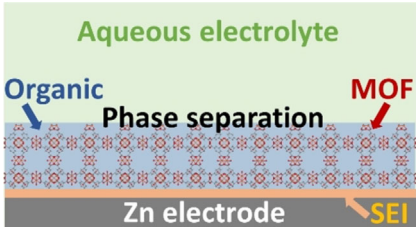

A highly reversible Zn anode is achieved by using a phase-separation electrolyte, where aqueous electrolyte is separated from Zn by a MOF-confined thin layer hydrophobic $Zn(TFSI)_2$-TFEP organic electrolyte and a ZnF_2-$Zn_3(PO_4)_2$ solid electrolyte interphase (SEI). The Zn anode achieves a high Coulombic efficiency of 99.9% at 1 mA cm^{-2} for 350 cycles and stable Zn||MnO_2 batteries.